Study of the Applicability of Fe Nanotubes as an Anode Material of Lithium-Ion Batteries

Artem L. Kozlovskiy[1, 2, *], Maxim V. Zdorovets[1, 3, 4],
Alena E. Shumskaya[5], and Kayrat K. Kadyrzhanov[3]

Abstract—The paper presents the results of the use of iron nanotubes as the anode material of lithium-ion batteries. To assess the degradation of the morphology of nanostructures after different numbers of cycles of life tests, the method of scanning electron microscopy, Mossbauer spectroscopy, and X-ray diffraction analysis were applied. It is shown that the decrease in discharge capacity starts at the 380th cycle and is caused by the onset of degradation processes of nanostructures due to the formation of amorphous inclusions and an increase in macrostresses and distortions in the structure. The complete degradation of the structure is observed after the 492nd life cycle test. According to the data obtained by Mossbauer spectroscopy, it has been established that an increase in life cycles leads to an increase in contribution of partial spectrum characteristic of a paramagnetic state. That indicates an increase in degradation rate of nanostructures and an increase in the content of impurity inclusions and amorphous formations in the crystal structure.

1. INTRODUCTION

Today, the big interest in nanoscale structures and devices based on them is due to their ability to control physical-chemical properties, as well as the size and shape [1–3]. The fabrication and control of nanoscale structures synthesized from a wide range of materials are crucial in the technological aspects and operation of nanostructured materials. Potential applications of nanostructures range from magnetic recording to bio-magnetism sensors and bases for lithium-ion batteries [4–6]. In the modern world, the main direction of the development of lithium-ion battery technology is associated with the achievement of higher energy density, increase in service life, reducing charging time, and increasing safety during operation. One of the ways to solve these problems is the development of new materials for electrodes and electrolytes [7–9]. Despite the active use of carbon and silicon nanostructures that have proven themselves as anode materials for lithium-ion batteries, due to the high stability and longer service life, there are a number of technological limitations on their production and control of structural properties [10–12]. Among the nanostructured materials, Fe-based nanostructures are attractive because of their excellent ferromagnetic properties, high level of magnetization, and ability to control the magnetic texture, which is one of the important characteristics for the potential use of nanostructures in various fields [13–18]. However, the possibility of a simple method of obtaining large arrays of nanostructures with controlled geometric and structural characteristics makes iron nanostructures a promising material for the base of lithium-ion batteries. Despite the huge interest in magnetic nanostructures and their use as cathode materials for lithium-ion batteries, there are many

questions related to the appropriateness and effectiveness of their use. So it is known that one of the most promising materials is nanostructures based on nickel and copper [19–24], which have proven themselves as an anode material quite well. It is also known that oxide forms of iron have great potential for use in this field [25–27], which is based on accelerated lithiation processes due to compounds of lithium ions with oxygen ions. However, the oxide form of iron nanostructures leads to an accelerated process of amorphization and destruction of particles or wires, due to weak chemical and crystalline bonds in the structure. In turn, iron nanotubes that do not contain oxide impurities in the initial state and have a developed morphology and a large specific surface can have a significant increase in the lifetime of nanostructures as anode materials.

The paper presents the results of a study of the applicability of iron nanostructures in the form of hollow nanotubes, as the basis for the anode material of lithium-ion batteries. As a method for producing nanostructures, the method of electrochemical synthesis was used. That makes it possible to fairly easily control the geometry and structural characteristics of synthesized nanostructures [28–31].

2. EXPERIMENTAL PART

Track membrane with a pore density of $4 \cdot 10^7$ pores/cm^2 with cylindrical pores with a diameter of $\sim 380 \pm 10$ nm was used as template matrices. The choice of the method of electrochemical deposition is due to the simplicity of scaling and the ability to control the physical-chemical properties of the synthesized nanostructures [32, 33].

Electrochemical deposition of PET template in a nanopore was carried out in a potentiostatic mode with a potential difference of 1.75 V. The composition of the electrolyte solution to produce iron nanostructures: 7-aqueous ferrous sulfate $FeSO_4 \times 7H_2O$, boric (H_3BO_3) and ascorbic ($C_6H_8O_6$) acids. All chemical reagents used were of reagent grade or analytical grade. The growth of nanostructures was monitored by chronoamperometry using an Agilent 34410A multimeter.

The study of the structural characteristics and elemental composition of nanotubes was carried out using a Hitachi TM3030 scanning electron microscope with a Bruker XFlash MIN SVE microanalysis system with an accelerating voltage of 15 kV. X-ray diffraction (XRD) analysis was performed on a D8 ADVANCE ECO diffractometer (Bruker, Germany) using CuKα radiation ($\lambda = 1.54060$ Å). BrukerAXSDIFFRAC.EVAv.4.2 software and the ICDD PDF-2 international database were used to identify the phases and study the crystal structure.

Mossbauer studies were carried out using an MS1104Em spectrometer operating in a constant acceleration mode with a triangular shape changing the Doppler velocity of the source relative to the absorber. The source was the ^{57}Co nuclei in the Rh matrix. The Mossbauer spectrometer was calibrated at room temperature using a standard α-Fe absorber. For processing and analyzing the Mossbauer spectra, methods were used to restore the distributions of the hyperfine parameters of the Mossbauer spectrum, taking into account a priori information about the object of study, implemented in the SpectrRelax program [34, 35].

Electrochemical testing of copper nanostructures was carried out in two-electrode CR20 32 cells on a charge-discharge test bench CT-3008W-5V (Neware company). Metallic lithium was used as a counter electrode. The electrolyte solution was a mixture of 1 M LiPF$_6$ ethylene carbonate/propylene carbonate/diethyl carbonate/ethyl methyl carbonate/propyl acetate. Anode cycling was carried out in galvanostatic mode in the voltage range from 10 mV to 2 V, in the mode of limiting the charging capacity of 1000 mA h/g. In the anode cycle, limiting was the achievement of 2 V voltage [22, 23].

3. RESULTS AND DISCUSSION

Figure 1 shows the SEM images and XRD pattern of the nanostructures obtained.

According to the data obtained, the studied nanostructures are hollow nanotubes with a length of 12 μm and an outer diameter of 380 nm. Using the method of XRD analysis, it was found that the samples under study are whisker-like structures with a textural direction of crystallite growth (110), a body-centered cubic lattice of the spatial syngony *Im-3m*(229) for the iron phase. The low-intensity peak in the region of $\theta = 54$–$55°$ corresponds to the polymer matrix, since the diffraction patterns were taken from the array of nanotubes in the matrix. Also, on the diffractogram obtained there are no
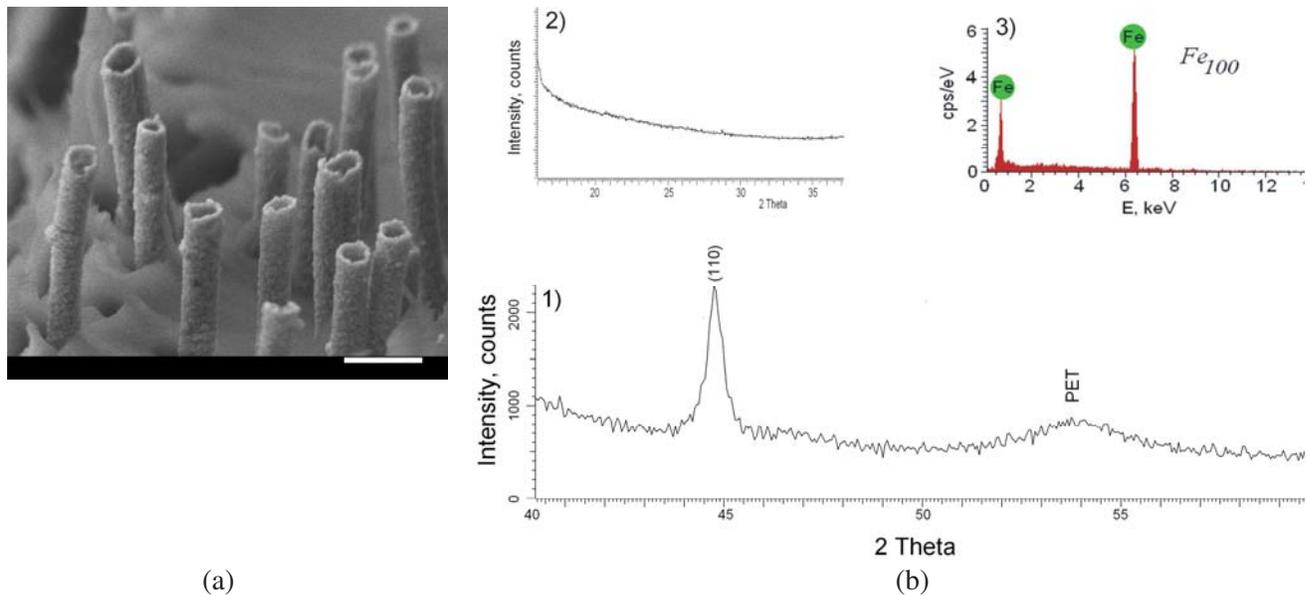
Figure 1. (a) SEM images of the nanostructures under study; (b) X-ray diffractogram of the studied nanostructures: 1) diffractogram in the range of $2\theta = 40–60°$; diffractogram in the range of $2\theta = 20–35°$; 3) EDA spectrum of the studied nanowires.

peaks characteristics of iron oxide compounds. The broadened and asymmetric form of the diffraction maximum (110) may be due to the presence of regions of disorder in the structure, as well as stresses and strains of the crystal lattice, which arise during nanotubes growth. The insets in Figure 1(b) show the X-ray diffractogram of the original nanotubes in the range of $2\theta = 20–40°$ and the energy dispersive spectrum. As can be seen from the presented data, no diffraction peaks are observed in the range of $2\theta = 20–40°$, which indicates the absence of oxide inclusions in the structure of the samples under study. Also, according to the data of energy dispersive analysis, the nanotubes under study are composed of iron, and reflexes characteristics of oxygen in the range of $E = 0–1.5\,keV$ were not detected.

One of the areas of application of nanostructures in the form of tubes is their use as anode materials for lithium-ion rechargeable batteries of a new generation. The basis of the application is the ability to accumulate a large amount of lithium due to the large specific surface, high degree of crystallinity, etc. One of the standards for determining the working life of batteries is a decrease in capacity below 80% of nominal, as well as the resistance of the anode material to degradation during operation. Figure 2 presents the results of life tests of the samples under study.

According to the presented data, it can be seen that for the studied samples the degradation of the material manifests itself in the form of an abrupt onset of a fall in the capacitance value after the 380th cycle, and complete degradation occurs at the 492nd cycle (the capacity decreases by more than 80% of the nominal). A sharp drop in capacity may be due to amorphization and partial degradation of nanostructures. In the future, the points corresponding to the beginning of the decline (380 cycles), the middle of the decline (450 cycles), and the achievement of the minimum value of the discharge capacity and complete degradation (492 cycles) were chosen as the points studied.

To assess the degradation of the morphology of nanostructures after a different number of cycles of life tests, the method of scanning electron microscopy was used. Figure 3 shows the SEM images of the dynamics of changes in the morphology of nanostructures.

As can be seen from the presented data, the beginning of the discharge capacity decline is associated with the onset of growth on nanotubes walls, which leads to a partial destruction of nanotubes structure. The increase in cycling leads to the formation of a large number of amorphous inclusions in the structure of nanotubes. For 492 cycles, which are characterized by the maximum drop in discharge capacity, nanotubes surface is covered with feather growths, which indicates a complete degradation of the structure. Evaluation of changes in the magnetic properties and the content of impurity inclusions
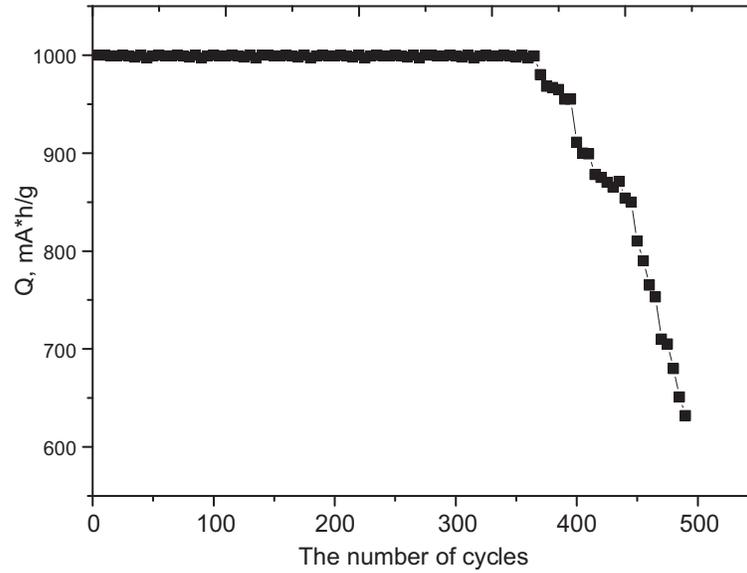
Figure 2. Graph of specific discharge capacity versus the number of cycles tested in charge capacity 1000 mA h/g.
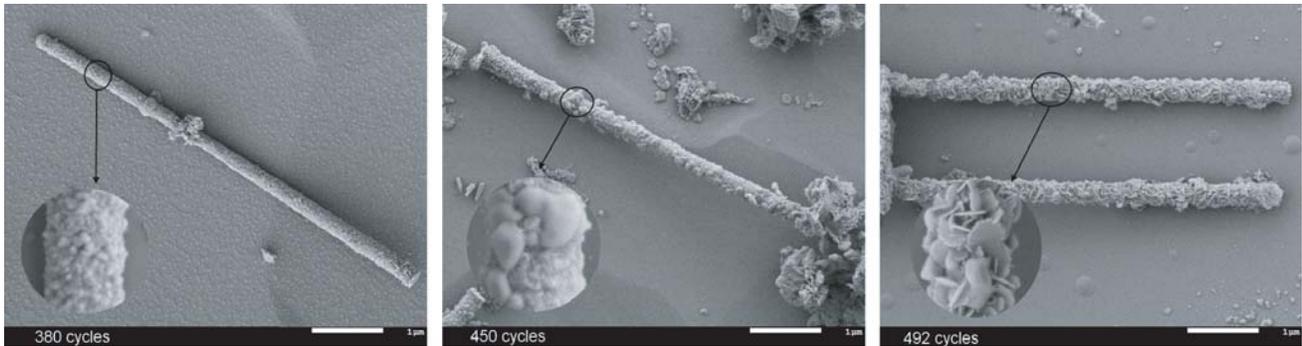

Figure 3. SEM images of the dynamics of changes in the morphology of nanostructures after life tests.

during the cycling process were carried out using the Mossbauer spectroscopy method. The results of changing the Mossbauer spectra are presented in Figure 4.

As can be seen from the presented data for initial nanotubes, the resulting spectrum is a Zeeman sextet and a low-intensity quadrupole doublet, characteristic of the paramagnetic state of the Fe^{2+} and Fe^3 cations. The presence of a quadrupole doublet indicates the presence of impurity inclusions in the structure. That leads to disordering of the magnetic texture, as well as the presence of a small number of cationic vacancies in the crystal structure, which confirms the results of XRD of investigated sample. An increase in the life cycle cycles leads to an increase in the contribution of the partial spectrum characteristic of a paramagnetic state. That indicates an increase in degradation rate of nanostructures and an increase in the content of impurity inclusions and amorphous formations in the crystal structure. The dynamics of changes in the contributions of partial spectra are presented in Figure 5.

It is known that in the Mossbauer spectrum of ^{57}Fe nuclei, the intensity ratio of the resonant lines of the Zeeman sextet depends on the angle between the direction of the gamma quantum span and the hyperfine magnetic field on the core (magnetic moment of the Fe atom)

$$\frac{I_{2,5}}{I_{1,6}} = \frac{4\sin^2\vartheta}{3(1+\cos^2\vartheta)}, \tag{1}$$

where $I_{2.5}$, $I_{1.6}$ are the intensities of the second and fifth, and the first and sixth lines in the sextet.
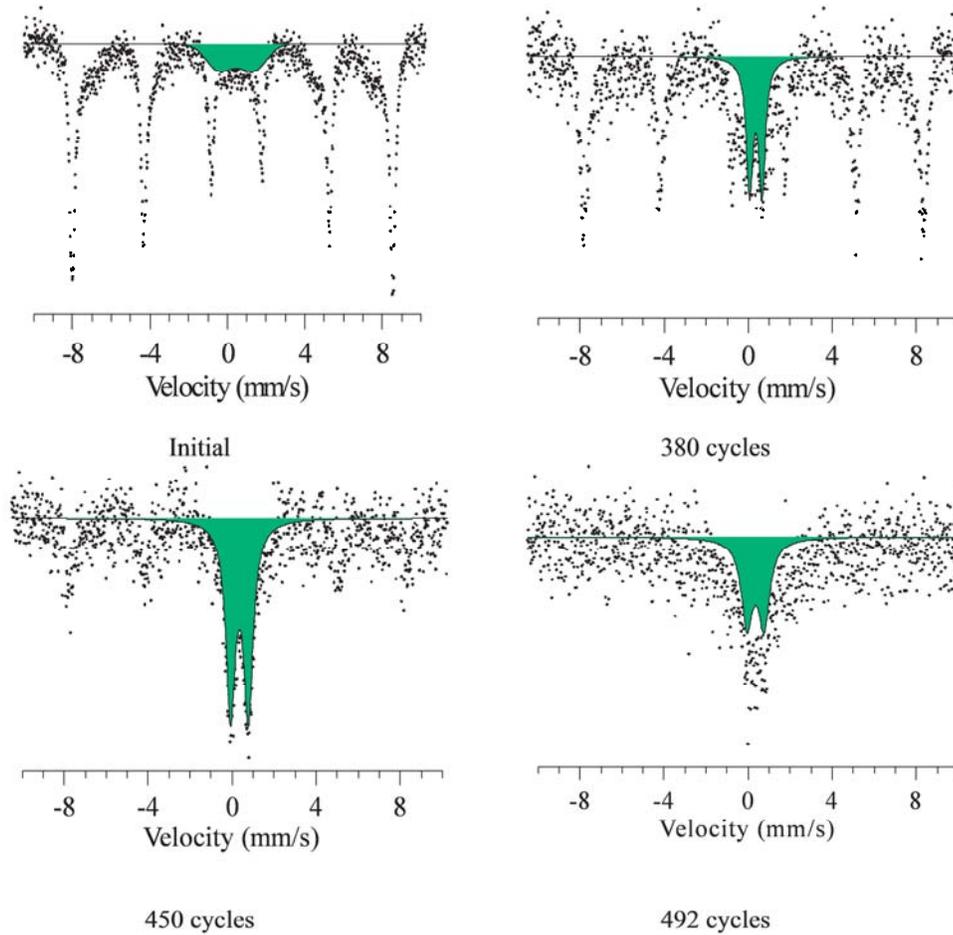
Figure 4. Mossbauer spectra of the studied nanotubes before and after the life test.

Figure 6 shows a plot of the change in the magnitude of the hyperfine magnetic field and the average value of the angle θ on the life test cycle.

The magnitude of the hyperfine magnetic field for the initial sample is 333.84 kOe, and the values of the shift δ of the Mossbauer line and the quadrupole shift ε for the Zeeman sextet are close to zero, which is characteristic of the α-Fe structure. An increase in the number of cycles, leading to an increase in the contribution of the paramagnetic doublet, leads to a sharp decrease in the magnitude of the hyperfine field. That is caused by an increase in the structure of amorphous inclusions and stresses in the crystal structure. In this case, a decrease in the magnitude of the hyperfine field and an increase in the contribution of the paramagnetic doublet lead to a disordered magnetic texture in samples.

Table 1 presents the changes in the main crystallographic characteristics before and after the life tests.

Table 1. Data on crystallographic characteristics.

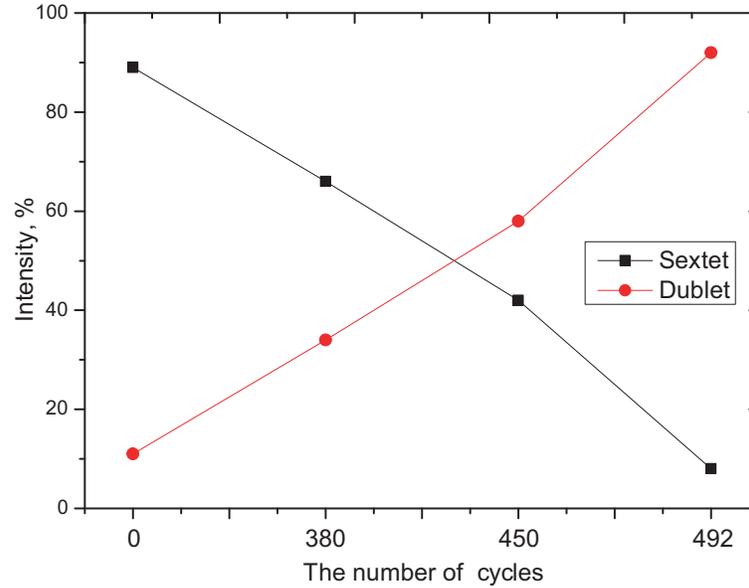| The number of cycles	Crystallographic characteristics		
	Lattice parameter, Å	The average crystallite size, nm	Density, g/cm^3
Initial	2.8593	22.1 ± 2.2	7.931
380	2.8604	18.2 ± 2.4	7.923
450	2.8692	14.7 ± 1.7	7.851
492	2.8754	9.5 ± 1.2	7.801

Figure 5. Dynamics of changes in the intensities of partial spectra depending from the synthesis conditions.
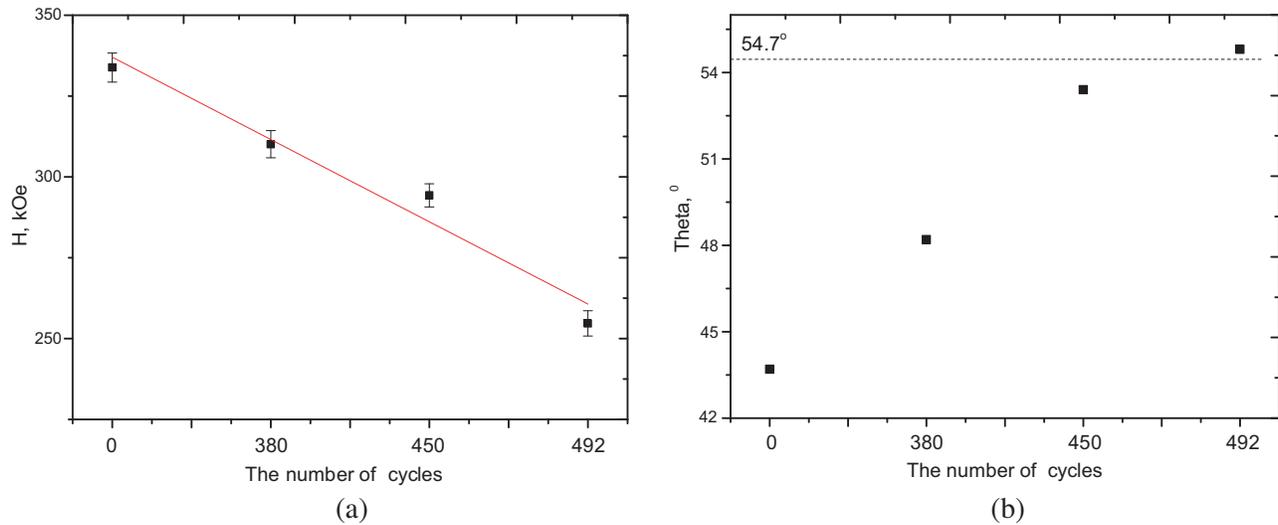

(a)   (b)

Figure 6. (a) Dynamics of change in the magnitude of the hyperfine magnetic field; Graph of changes in the average value of the angle θ. (The line on the graph shows the characteristic value for the absence of ordering of magnetic moments).

As can be seen from the presented data, an increase in the number of cycles leads to an abrupt change in the lattice parameters and nanotube density. That may be due to the partial destruction of chemical bonds in the structure as a result of degradation and the introduction of impurity inclusions in the lithiation process. The decrease in the average crystallite size indicates the processes of crushing and destruction of the crystal structure, leading to degradation and decrease in performance. Based on the obtained diffractograms, the Rietveld method was used to determine the change in the content of impurity inclusions in the structure. Determination of the volume fraction of the contribution of the impurity phases was carried out using Equation (2):

$$V_{\text{admixture}} = \frac{RI_{\text{phase}}}{I_{\text{admixture}} + RI_{\text{phase}}} \tag{2}$$

I_{phase} is the average integrated intensity of the main phase of the diffraction line, Ia_{dmixture} the average integrated intensity of the additional phase, and R the structural coefficient equal to 1.45. Figure 7(a) shows the X-ray diffractograms of the samples under study after series of life tests. As can be seen from the presented data, an increase in the number of test cycles leads to a decrease in the intensity and asymmetric distortion of the diffraction maximum (110), as well as the appearance of peaks characteristic of oxide inclusions in the range of $2\theta = 35$–$40°$, which confirms Mössbauer spectroscopy data. Figures 7(b)–(c) present the results of changes in the concentration of amorphous inclusions in the structure and macrostresses after life tests, calculated on the basis of XRD data.
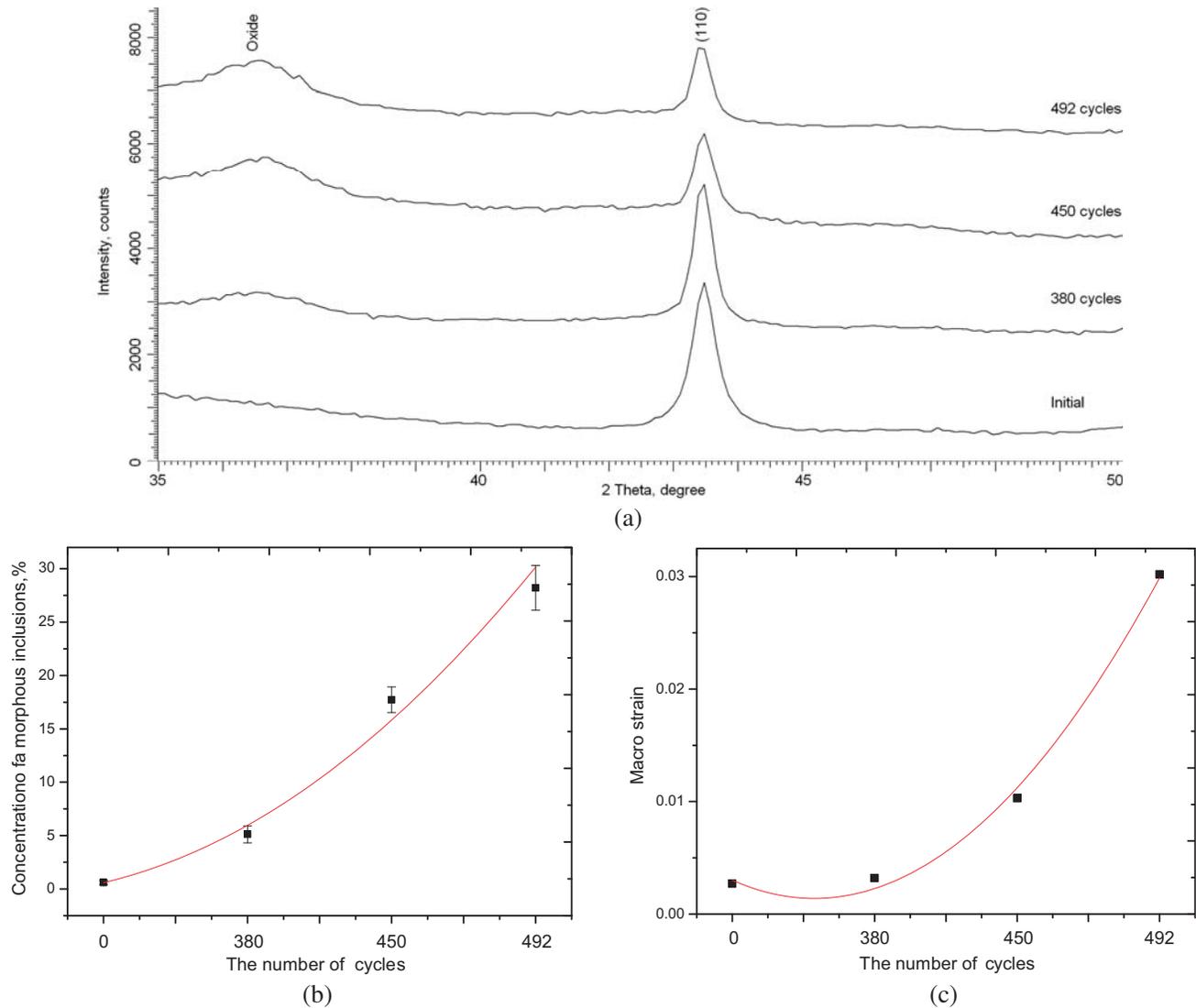

Figure 7. (b) Graph of changes in the concentration of amorphous inclusions in the structure of nanotubes before and after the life test; (c) Graph of changes in macrostresses in the structure.

The obtained data on changes in the concentration of amorphous inclusions and macrostresses in the structure confirm the data of Mossbauer spectroscopy and scanning electron microscopy. A sharp increase in macrostresses and the content of amorphous inclusions leads to uncontrolled degradation of the structure, a decrease in density and partial destruction. That leads to a decrease in discharge capacity and deterioration in the performance of nanotubes.

4. CONCLUSION

The paper presents the results of the use of iron nanotubes as the anode material of lithium-ion batteries. The resource lifetime to complete degradation has amounted to 492 cycles in the mode of limiting the charging capacity of 1000 mA h/g, which is used in most lithium-ion batteries. It is shown that the decrease in the discharge capacity starts at the 380th cycle and is caused by the onset of the processes of degradation of nanostructures due to the formation of amorphous inclusions and an increase in macrostresses and distortions in the structure. The increase in cycling leads to the formation of a large number of amorphous inclusions in the structure of nanotubes. For the 492nd cycle, which is characterized by the maximum drop in discharge capacity, the nanotubes surface is covered with feather growths, which indicates a complete degradation of the structure.

The ease of manufacture and uniformity in the composition and properties of iron nanostructures make them promising materials for anodes of lithium-ion batteries and modern batteries.

REFERENCES

1. Lahiri, I. and W. Choi, "Carbon nanostructures in lithium ion batteries: Past, present, and future," *Critical Reviews in Solid State and Materials Sciences*, Vol. 38, No. 2, 128–166, 2013.
2. Xia, T., et al., "Facile complex-coprecipitation synthesis of mesoporous Fe_3O_4 nanocages and their high lithium storage capacity as anode material for lithium-ion batteries," *Electrochimica Acta*, Vol. 160, 114–122, 2015.
3. Liu, J., et al., "A flexible alkaline rechargeable Ni/Fe battery based on graphene foam/carbon nanotubes hybrid film," *Nano Letters*, Vol. 14, No. 12, 7180–7187, 2014.
4. Kozlovskiy, A., et al., "Mossbauer research of Fe/Co nanotubes based on track membranes," *Nuclear Instruments and Methods in Physics Research Section B: Beam Interactions with Materials and Atoms*, Vol. 381, 103–109, 2016.
5. Wu, Q., et al., "Microwave absorption and mechanical properties of cross-scale SiC composites," *Composites Part B: Engineering*, Vol. 155, 83–91, 2018.
6. Shanbedi, M., et al., "Effect of magnetic field on thermo-physical and hydrodynamic properties of different metals-decorated multi-walled carbon nanotubes-based water coolants in a closed conduit," *Journal of Thermal Analysis and Calorimetry*, Vol. 131, No. 2, 1089–1106, 2018.
7. Zakaria, M. R., et al., "Comparative study of graphene nanoparticle and multiwall carbon nanotube filled epoxy nanocomposites based on mechanical, thermal and dielectric properties," *Composites Part B: Engineering*, Vol. 119, 57–66, 2017.
8. Lobiak, E. V., et al., "Structure and electrochemical properties of carbon nanotubes synthesized with catalysts obtained by decomposition of Co, Ni, and Fe polyoxomolybdates supported by MgO," *Journal of Structural Chemistry*, Vol. 59, No. 4, 786–792, 2018.
9. Cheng, H.-M., C. Liu, and P.-X. Hou, "Field emission from carbon nanotubes," *Nanomaterials Handbook*, 255–272, 2nd Edition, CRC Press, 2017.
10. Shirvanimoghaddam, K., et al., "Carbon fiber reinforced metal matrix composites: Fabrication processes and properties," *Composites Part A: Applied Science and Manufacturing*, Vol. 92, 70–96, 2017.
11. Rusakov, V. S., et al., "A Mössbauer study of iron and iron-cobalt nanotubes in polymer ion-track membranes," *Moscow University Physics Bulletin*, Vol. 71, No. 2, 193–201, 2016.
12. Chen, C. and X. Wang, "Adsorption of Ni (II) from aqueous solution using oxidized multiwall carbon nanotubes," *Industrial & Engineering Chemistry Research*, Vol. 45, No. 26, 9144–9149, 2006.
13. Kadyrzhanov, K. K., V. S. Rusakov, A. L. Kozlovskiy, M. V. Zdorovets, E. Y. Kaniukov, A. E. Shumskaya, I. E. Kenzhina, and M. S. Fadeev, "Structural and magnetic studies of Fe_{100-X} Co_x nanotubes obtained by template method," *Progress In Electromagnetics Research C*, Vol. 82, 77–88, 2018.

14. Abukhadra, M. R., et al., "Superior removal of Co 2+, Cu 2+ and Zn 2+ contaminants from water utilizing spongy Ni/Fe carbonate-fluorapatite; preparation, application and mechanism," *Ecotoxicology and Environmental Safety*, Vol. 157, 358–368, 2018.

15. Shumskaya, A. E., E. Y. Kaniukov, A. L. Kozlovskiy, D. I. Shlimas, M. V. Zdorovets, M. A. Ibragimova, V. S. Rusakov, and K. K. Kadyrzhanov, "Template synthesis and magnetic characterization of FeNi nanotubes," *Progress In Electromagnetics Research C*, Vol. 75, 23–30, 2017.

16. Korolkov, I. V., et al., "Immobilization of carborane derivatives on Ni/Fe nanotubes for BNCT," *Journal of Nanoparticle Research*, Vol. 20, No. 9, 240, 2018.

17. Sellmyer, D. J., M. Zheng, and R. Skomski, "Magnetism of Fe, Co and Ni nanowires in self-assembled arrays," *Journal of Physics: Condensed Matter*, Vol. 13, No. 25, R433, 2001.

18. Paulo, V. I. M., et al., "Magnetization curves of electrodeposited Ni, Fe and Co nanotubes," *Materials Letters*, Vol. 223, 78–81, 2018.

19. Taberna, P.-L., et al., "High rate capabilities Fe_3O_4-based Cu nano-architectured electrodes for lithium-ion battery applications," *Nature Materials*, Vol. 5, No. 7, 567, 2006.

20. Kozlovskiy, A. and M. Zdorovets, "Study of the applicability of directional modification of nanostructures to improve the efficiency of their performance as the anode material of lithium-ion batteries," *Materials Research Express*, Vol. 6, No. 7, 075066, 2019.

21. Kozlovskiy, A., et al., "Effect of irradiation with C 2+ and O 2+ ions on the structural and conductive characteristics of copper nanostructures," *Materials Research Express*, Vol. 6, No. 7, 075072, 2019.

22. Chen, Z., et al., "Carbon particles modified macroporous Si/Ni composite as an advanced anode material for lithium ion batteries," *International Journal of Hydrogen Energy*, Vol. 44, No. 2, 1078–1087, 2019.

23. Li, Q., et al., "Porous nitrogen-doped carbon nanofibers assembled with nickel nanoparticles for lithium-sulfur batteries," *Nanoscale*, Vol. 11, No. 2, 647–655, 2019.

24. Shlimas, D. A., et al., "Study of the use of ionizing radiation to improve the efficiency of performance of nickel nanostructures as anodes of lithium-ion batteries," *Materials Research Express*, Vol. 6, No. 5, 055026, 2019.

25. Lee, S. H., et al., "Self-assembled Fe_3O_4 nanoparticle clusters as high-performance anodes for lithium ion batteries via geometric confinement," *Nano Letters*, Vol. 13, No. 9, 4249–4256, 2013.

26. Wang, J.-Z., et al., "Graphene-encapsulated Fe_3O_4 nanoparticles with 3D laminated structure as superior anode in lithium ion batteries," *Chemistry — A European Journal*, Vol. 17, No. 2, 661–667, 2011.

27. He, C., et al., "Carbon-encapsulated Fe_3O_4 nanoparticles as a high-rate lithium ion battery anode material," *ACS Nano*, Vol. 7, No. 5, 4459–4469, 2013.

28. Wang, F., et al., "Microwave absorption properties of 3D cross-linked Fe/C porous nanofibers prepared by electrospinning," *Carbon*, Vol. 134, 264–273, 2018.

29. Torres, D., J. Pinilla, and I. Suelves, "Co-, Cu- and Fe-doped Ni/Al_2O_3 catalysts for the catalytic decomposition of methane into hydrogen and carbon nanofibers," *Catalysts*, Vol. 8, No. 8, 300, 2018.

30. Li, Y., et al., "Annealing effects on the microstructure, magnetism and microwave-absorption properties of Fe/TiO_2 nanocomposites," *Journal of Magnetism and Magnetic Materials*, Vol. 471, 346–354, 2019.

31. Azab, A. A., E. E. Ateia, and S. A. Esmail, "Comparative study on the physical properties of transition metal-doped (Co, Ni, Fe, and Mn) ZnO nanoparticles," *Applied Physics A*, Vol. 124, No. 7, 469, 2018.

32. Kurakhmedov, A. E., et al., "Asymmetrical track-etched membranes prepared by double-sided irradiation on the DC-60 cyclotron," *Petroleum Chemistry*, Vol. 57, No. 6, 489–497, 2017.

33. Kaniukov, E. Y., et al., "Evolution of the polyethylene terephthalate track membranes parameters at the etching process," *Journal of Contemporary Physics (Armenian Academy of Sciences)*, Vol. 52,

No. 2, 155–160, 2017.

34. Matsnev, M. E. and V. S. Rusakov, "SpectrRelax: An application for Mössbauer spectra modeling and fitting," *AIP Conference Proceedings*, Vol. 1489, No. 1, AIP, 2012.

35. Kozlovskiy, A., et al., "Study of Ni/Fe nanotube properties," *Nuclear Instruments and Methods in Physics Research Section B: Beam Interactions with Materials and Atoms*, Vol. 365, 663–667, 2015.